Journal of Nanoparticle Research (2007) 9:365–375
DOI 10.1007/s11051-006-9141-2

Research Paper

Preparation of N-doped TiO_2 photocatalyst by atmospheric pressure plasma process for VOCs decomposition under UV and visible light sources

Chienchih Chen[1], Hsunling Bai[1,*], Sue-min Chang[1], Chungliang Chang[2] and Walter Den[3]
[1]*Institute of Environmental Engineering, National Chiao Tung University, Hsinchu, Taiwan;* [2]*Department of Environmental Engineering and Health, Yuanpei Institute of Science and Technology, Hsinchu, Taiwan;* [3]*Department of Environmental Science and Engineering, Tunghai University, Taichung, Taiwan; *Author for correspondence (Tel.: +886-3-573-1868; Fax: +886-3-572-5958; E-mail: hlbai@mail.nctu.edu.tw)*

Received 5 March 2006; accepted in revised form 30 June 2006

Key words: titania, photocatalytic reaction, plasma process, dielectric barrier discharge, nitrogen doping, visible light irradiation, isopropanol, toluene, nanoparticles

Abstract

The nitrogen doped (N-doped) titanium dioxide (TiO_2) photocatalyst was prepared by the atmospheric-pressure plasma-enhanced nanoparticles synthesis (APPENS) process operated under normal temperature, i.e. the dielectric barrier discharge plasma process. The N_2 carrier gas is dissociated in the AC powered nonthermal plasma environment and subsequently doped into the TiO_2 photocatalyst that was capable of being induced by visible light sources. The APPENS process for producing N-doped TiO_2 showed a higher film deposition rate in the range of 60–94 nm/min while consuming less power (< 100 W) as compared to other plasma processes reported in literatures. And the photocatalytic activity of the N-doped TiO_2 photocatalyst was higher than the commercial ST01 and P25 photocatalysts in terms of toluene removals in a continuous flow reactor. The XPS measurement data indicated that the active N doping states exhibited N 1s binding energies were centered at 400 and 402 eV instead of the TiN binding at 396 eV commonly observed in the literature. The light absorption in the visible light range for N-doped TiO_2 was also confirmed by a clear red shift of the UV-visible spectra.

Introduction

Photocatalysis of volatile organic compounds (VOCs) is one of the most popular indoor and outdoor air pollution control approaches because of its low energy consumption. However, most of the studies have been focused on the utilization of light sources in the ultraviolet (UV) spectrum with titanium dioxide (TiO_2) as the photocatalysts (Fujishima et al., 2000). In the recent years, a number of studies (Asahi et al., 2001; Ohno et al., 2004) have reported that doping TiO_2 with metal or non-metal compounds could initiate photo activation by visible light sources, thereby improving VOCs destruction efficiency and potentially expanding its fields of application. Among the viable doping elements or compounds for TiO_2, the substitutional doping of N has been recognized to be one of the most effective means for producing visible light irradiation effect (Asahi et al., 2001; Ihara et al., 2003; Irie et al., 2003).

Many methods have been documented to successfully prepare N-doped TiO_2 films or particles, including surface treatment by sputtering (Asahi et al., 2001) or plasma (Miao et al., 2004), pulsed laser deposition (György et al., 2003; Suda et al.,

2005), sol–gel (Livraghi et al., 2005) or other aqueous phase reactions (Sakatani et al., 2004; Chen et al., 2005; Nosaka et al., 2005; Yin et al., 2005), and the plasma-assisted deposition processes. The plasma-assisted processes, such as ion-beam-assisted deposition (IBAD) (Yang et al., 2004a; Yang et al., 2004b; Wu et al., 2005) and the radio frequency (r.f.) plasma-enhanced chemical vapor deposition (PECVD) (Battison et al., 2000; Irie et al., 2003; Maeda and Watanabe, 2006) for the preparation of TiO_2, own numerous advantages such as high product purity, excellent step coverage, and precise control of reaction parameters (Battison et al., 2000). However, most of the plasma processes entail stringent operating environment of low pressures (vacuum) and/or high temperatures.

In a previous study, the present authors have successfully produced uniform and nano-size particles by an atmospheric-pressure nonthermal plasma process, hereafter referred as APPENS (atmospheric-pressure plasma-enhanced nanoparticles synthesis) process (Bai et al., 2004). As compared to other plasma processes, the APPENS process holds a distinct advantage in three-folds: (i) it operates without requiring environments with near vacuum or elevated temperature conditions, (ii) the energy requirement is low but sufficient for breaking and doping N_2 or NH_3 molecules into the titania precursors, and (iii) the plasma source of the APPENS process has been widely applied for industrial ozone production, therefore scaling up of the system for the mass production of N-doped TiO_2 nano-films or nano-particles appears highly viable.

In the present study, the N-doped TiO_2 photocatalytic nano-particles were prepared and utilized to decompose toluene and isopropanol (IPA), two VOCs commonly existed in the industrial emissions as well as in the indoor ambiences. The effectiveness of the prepared photocatalyst was examined under UV and visible light sources, and was subsequently compared with the performances by the bare anatase TiO_2 and the commercial photocatalysts as well. The production rate of photocatalysts and the energy requirement of the process were also evaluated in the context of other plasma processes available in literatures.

Experimental

Preparation of N-doped TiO_2 photocatalyst

A schematic diagram of the APPENS process for producing the N-doped photocatalyst is shown in Figure 1. The titanium tetraisoproxide (TTIP) and water vapor, both serving as the reaction precursors, were obtained by passing N_2 carrier gas into separate impingers controlled at 150 and 25 °C, respectively, before mixing and delivering into the plasma reactor. The plasma reactor was made of Pyrex glass with 21 mm I.D., 23 mm O.D. and 200 mm in length. The total flow rate of the precursor vapors was 137.4 sccm, with TTIP/H_2O volumetric flow ratio of 4.0 at 25 °C being the

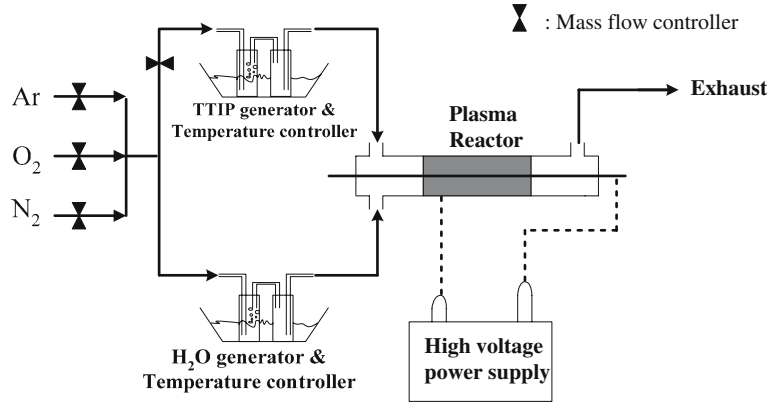

Figure 1. Schematic diagram of the APPENS reactor for producing N-doped TiO_2 nanoparticles.

optimal mixture as determined from the previous study (Bai et al., 2004).

The APPENS process was modified from a wire-tube type glow dielectric barrier discharge reactor. One electrode was a stainless steel rod of 2 mm in diameter positioned along the central line of the reactor. The other electrode was a sheet of stainless steel mesh wrapped around a portion of the reactor (135 mm in wrapping length). An alternative current (AC) with 60 Hz frequency was applied in the non-thermal plasma reactor, yielding an electric field strength of 9.6 kV/cm in atmospheric pressure. Under such conditions, the total power consumption of the process was approximately 9 W. The photocatalytic nanoparticles were either directly deposited on the reactor wall as a thin film or collected at the reactor outlet by a filter paper (A100A047A, Advantec MFS, Inc.) for further analysis.

After the plasma process, the glass tube was annealed at 500 °C in air for 3 h to remove carbon residue and to transform the titania from amorphous to anatase phase. To establish a basis for comparison, bare TiO_2 photocatalyst of pure anatase was also prepared via the APPENS process under the operation conditions identical to those used for preparing the N-doped TiO_2, except that the carrier gas of the plasma process as well as the annealing gas was $20\%O_2 + 80\%Ar$. The crystallite phase and size of the samples was determined by the X-ray diffraction patterns using an X-ray powder diffractometer (XRPD, Rigaku; Cu target, 30 kV, 20mA), with the results from transmission electron microscopy (TEM, Philips CM-200 TWIN) analysis, BET surface area measurement (ASAP 2020, Micromeritics) and SMPS (Scanning Mobility Particle Sizer, TSI model 3080L) measurement as the supporting evidence. In addition, the chemical composition of the N-doped TiO_2 was analyzed by electron spectroscopy for chemical analysis (ESCA, Perkin–Elmer; PHi 1600).

To facilitate quantitative comparisons concerning the production rate of TiO_2 photocatalysts between the APPENS and the other plasma processes, a plate-type plasma reactor capable of receiving a flat glass substrate of 50 mm in diameter was used. The power consumption of the plate-type reactor increased to 60–80 W, which was about 6–9 times higher than the wire-tube geometry. The N-doped TiO_2 film collected on the glass substrate was then weighed, and the film thickness was estimated based on the visual images taken by scanning electron microscopy (SEM, Hitachi-S4700).

Photocatalytic degradation of IPA in a batch reactor

A batch photocatalytic reactor for IPA and Toluene removal is sketched in Figure 2a. The reactor was essentially the same device as the one used for producing the TiO_2 particles, except that the inlet and outlet ends were sealed to form a batch-type configuration. Before the photocatalytic reaction test, small amounts of IPA 0.04 μL) and toluene (0.01 μL) were injected separately into the sealed reactor at a constant temperature of 45 °C and relative humidity of 70%. After 60 min, the IPA and toluene reached a steady-state vapor concentration of 145 ± 1 and 250 ± 10 ppm as confirmed by a GC/FID (China Chromatography, 9800). The illuminating light was then turned on and the concentrations of IPA or toluene vapors subjected to the photocatalytic decomposition by either the TiO_2 or the N-doped TiO_2 photocatalysts were recorded. To avoid the diffusion limitation in a batch reactor, the light was turned off for 30 min after each sampling to ensure well mixed of the organic molecules, and then the light was turned on again to continue the photocatalysis tests.

Photocatalytic degradation of toluene in a continuous flow reactor

In addition to the batch-type decomposition studies, continuous flow (Figure 2b) studies targeting toluene removal were also performed using 5 mm glass beads (Beco Mfg Corp.) as the packing media. The glass beads were directly coated with N-doped TiO_2 after 10 h of the plasma process. The BET surface area of the glass beads was determined (ASAP 2020, Micromeritics) to be 0.0278 m^2/g with negligible pores. The mass of the coated photocatalysts per clean glass beads was 1.17 mg/g, and the mass of photocatalyst per surface area of clean glass beads was 42.24 mg/m^2.

For comparison basis, approximately the same amounts ($\pm$ 0.07 mg/g) of ST01 and P25 photocatalysts as the N-doped TiO_2 were also coated on the glass beads and tested in separate reactors under the identical conditions. The commercial photocatalysts of ST01 (Ishihara Sangyo) and P25

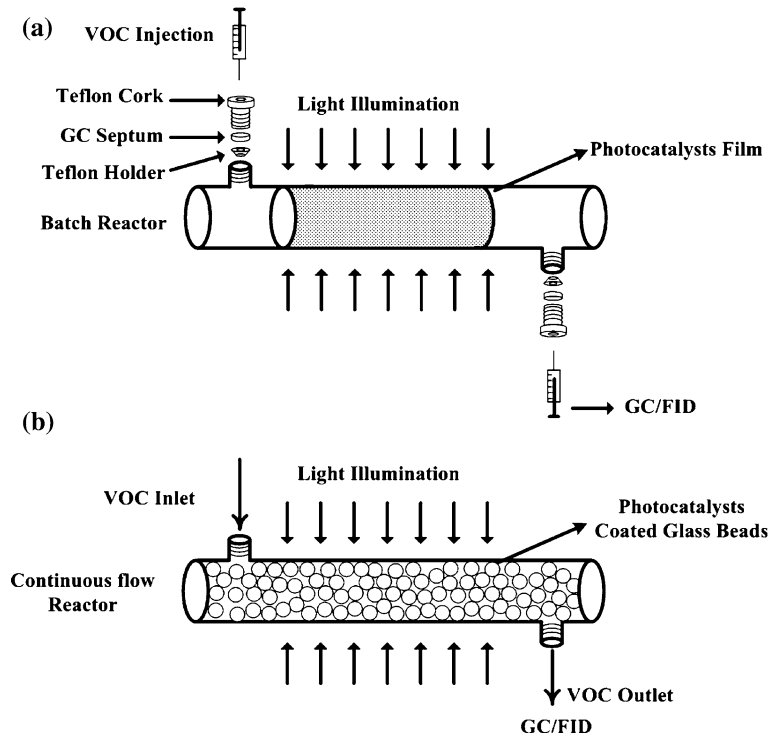

Figure 2. Schematics of the (a) batch type and (b) continuous flow photocatalytic reactors for VOCs removal.

(Degussa) powders were dispersed into the de-ionic water to a concentration of 50 g/L. Then the clean glass beads were dipped into the slurries and dried at 105 °. The glass beads were weighted before and after coating procedure to determine the actual coating amount of ST01 and P25 on the glass beads.

The toluene vapor was obtained from an impinger with clean air as the carrier gas, with the total gas flow rate of 18.3 sccm and typical toluene concentration of 463 ± 13 ppm. The reaction temperature and the relative humidity were maintained at 25 °C and 70%, respectively. The corresponding residence time in the continuous flow photocatalytic reactor was 2.35 min.

The illumination light sources used in the batch and continuous flow photocatalytic decomposition studies were either UV (364.2 nm; FL10BLB, Sankyo Denki) or visible light (FL10D-EX, Tyo Light) sources having the same irradiation intensity (10 W). To facilitate understanding of the prepared photocatalyst for indoor air pollution control application, the visible light bulb used in this study is simply the one used in household living space. Both the intensity and the spectra of the light sources were obtained from a spectrophotometer (Ocean Optics, USB2000). The intensities of illumination in the reactor were 3.78 mW/cm^2 for UV light source and 4.81 mW/cm^2 for visible light source. The light spectra of the visible light source are shown in Figure 3 with major peaks observed at 435, 488, 545, 587 and 611 nm. One can also observed a very small peak for visible light lamp at UV range of 364 nm with intensity of 0.35 mW/cm^2. To ensure the effect of this small peak at 364 nm on visible light photocatalysis, a photocatalysis test was also conducted with UV lamb (364.2 nm) of 0.43 mW/cm^2 intensity (a precise control of the light intensity to be 0.35 mW/cm^2 was not feasible during the test). And the results revealed that both the IPA and toluene removals were below detection limit.

Blank tests were conducted for both batch and continuous flow photocatalytic tests. The blank tests included those conducted with catalyst but without illumination, and those without catalyst but with light illumination. Each type of blank tests showed that the removals of IPA and toluene vapors are negligible.

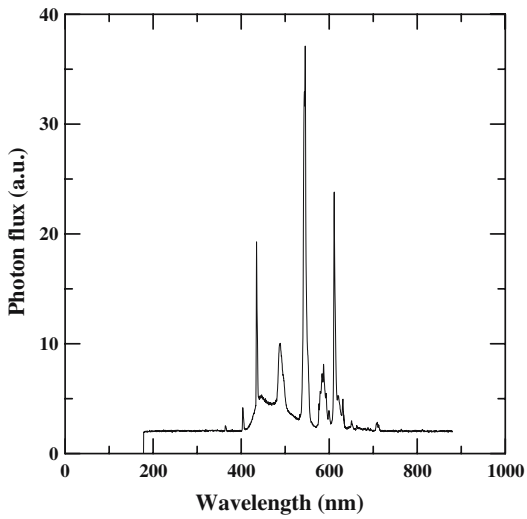

Figure 3. The light spectra of the visible light source used in this study. The three major peaks were observed at 435, 488, 545, 587 and 611 nm.

Results and discussion

Comparison of the APPENS process with other plasma processes

Values of the operating parameters and the basic properties of the N-doped TiO_2 prepared via the APPENS process are summarized in Table 1. These values are compared to the available literature data which employed other plasma processes for producing N-doped TiO_2 photocatalysts, namely the ion-beam-assisted deposition (IBAD) and the r.f. plasma-enhanced chemical vapor deposition (PECVD) processes.

As a common feature of all plasma processes, the particles produced by the APPENS process were firmly coated on the reactor surface and could not be easily removed by mechanical or chemical washing. Therefore it was possible that the TiO_2 vapors were deposited onto the reactor surface (i.e. via CVD process) first and then crystallized to form TiO_2 particles. Besides, the APPENS process also produced high quality films in terms of uniform size within nano-range as well as high photo-reactivity as demonstrated hereafter in this study.

In addition to the common feature of firm coating and high quality films among all plasma processes, the APPENS process was operative under normal conditions (i.e., room temperature and atmospheric pressure) as opposed to the IBAD and the PECVD processes. Therefore, the photocatalyst prepared by the APPENS process could be deposited on a substantially wider variation of substrate materials. Furthermore, the power consumption of the APPENS process (< 80 W)

Table 1. The operation parameters and the product properties of the APPENS process and other plasma processes for producing N-doped TiO_2 photocatalysts.

Properties	APPENS (This study)	Reference processes	
		IBAD (Yang et al., 2004a, b; Wu et al., 2005)	PECVD (Battison et al., 2000)
System temperature	298 K	523–573 K	393–523 K
Temperature of TTIP	423 K	Not available	313 K
System pressure	~101,300 Pa (i.e. ~1 atm)	10^{-4}–10^{-2} Pa	60 Pa
Power	Wire tube: ~9 W; Plate: 60–80 W	3 kW (Wu et al., 2005)	10500 W
Gas flow rate	137.4 sccm	< 20 sccm	20 sccm
Production rate	60–94 nm/min (plate type)	6–12 nm/min	< 10–25 nm/min
Grain size	~12 nm (25 nm)[a]	20–200 nm	20–30 nm
Crystal phase	Amorphous, then to anatase after 3 h annealing at 773 K	Direct use of anatase source (Wu et al., 2005). Rutile TiO_2 source material transferred to amorphous or anatase (Yang et al., 2004a, b)	Amorphous, then to anatase after 6 h annealing at 773 K.

[a]The grain size was around 12 nm as estimated by the Scherrer equation (Musić et al., 1997) based on XRPD data and the particle size was around 25 nm as observed from TEM photo images for tests shown in this study. The particle size may vary from 20–40 nm as the precursor ratio and the applied voltage were varied in the APPENS process.

was less than that of the PECVD (100–500 W) and the IBAD (3 kW) processes.

The production rate of the N-doped photocatalyst was in the range of 60–94 nm/min as verified by the plate-type APPENS process, with a SEM photo image of the N-doped TiO_2 deposited on a glass substrate shown in Figure 4. This production rate is much greater than those exhibited by the IBAD and PECVD processes, most probably due to the higher gas flow rate of 137.4 sccm employed in this study as compared to those (~20 sccm) used in the IBAD and PECVD processes. It is also noted that although a direct comparison between the production rate of the wire-tube plasma reactor and those of the IBAD and PECVD processes was not feasible, the total mass production rate in the wire-tube plasma reactor as collected by the glass beads (8.3 ± 0.5 mg/h) was about 20 times greater than that in the plate-type plasma reactor (0.4 ± 0.05 mg/h). Hence the production rate of the APPENS reactor should be higher than that of the IBAD and PECVD process because scaling up of the IBAD and PECVD processes for operating at higher flow rates are technically not feasible due to the necessity of vacuum condition.

The TEM images (Bai et al., 2004) indicated that the product particles were very uniform in size, whether or not nitrogen was doped into the TiO_2 particles. The variation in the average diameters between 20 and 40 nm depended on the operating conditions such as the precursor ratio and the plasma intensity. The crystallite sizes were also calculated by the Scherrer equation (Musić et al., 1997) using data obtained from the XRPD pattern for the $TiO_{2-X}N_X$ nanoparticles. The calculation results showed that the crystallite sizes were 11.8 ± 0.5 nm for particles having an estimated average size of 25 nm based on 62 primary particles observed in the TEM images.

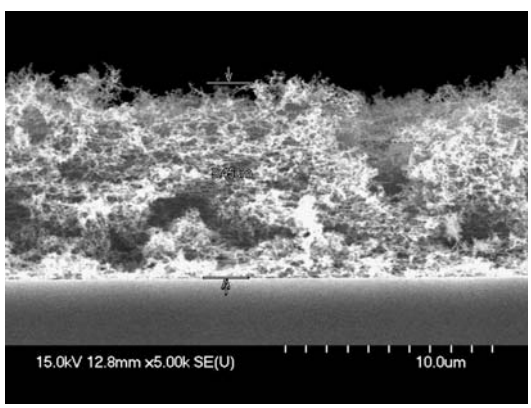

Figure 4. SEM photo image that shows the film thickness of N-doped TiO_2 deposited on a glass substrate via a plate type APPENS reactor. The electric field strength was 19.2 kV/cm and the deposition time was 2 h.

To check the difference between the TEM observed particle size and the XRPD-determined crystallite size, both SMPS (Scanning Mobility Particle Sizer, TSI model 3080L) and BET surface area (ASAP 2020, Micromeritics) measurements were conducted. The online measurement of the size distribution by SMPS indicated that the geometric standard deviation of the particle size distribution was around 1.21 at a particle size of 23 nm. While the powder specific surface area by nitrogen adsorption was determined to be 69.9 m^2/g, thus the specific surface area-determined particle size (d_p) was 22 nm using $d_p = 6/(\rho_p A)$, where ρ_p is the density of anatase TiO_2, and A is the BET specific surface area. Because there was no obvious porosity of the photocatalysts observed by the adsorption-desorption curve of BET measurement, one can conclude that the difference in TEM particle size and XRPD-determined crystallite size was mainly due to coagulation of crystallite particles.

The particles collected directly from the substrate via the APPENS process were amorphous, but they became strictly anatase after being annealed at 500 °C for 3 h. The anatase structure was observed regardless whether nitrogen was doped into TiO_2 photocatalysts.

Characterization of the N-doped TiO_2 photocatalyst

The evidence of the nitrogen doping is provided by the ESCA spectrometry of Ti 2p and N 1s, as shown in Figure 5. According to the literature database (Jill Ed., 1992), TiO_2 is characterized with peaks appearing at around 458–459 eV for Ti $2p_{3/2}$ and 464 eV for Ti $2p_{1/2}$. The presence of $TiO_{2-x}N_x$, however, tends to shift the Ti 2p peaks to lower binding energy (Miao et al., 2004; Chen et al., 2005). More importantly, the presence of N-doping in the TiO_2 particles is substantiated by the N 1s spectra, where a significant peak at around 402 eV and a minor peak at around 400 eV were observed for the photocatalysts doped with nitrogen. In contrast, there were no obvious N 1s peaks for the TiO_2 photocatalysts prepared in O_2/Ar environment.

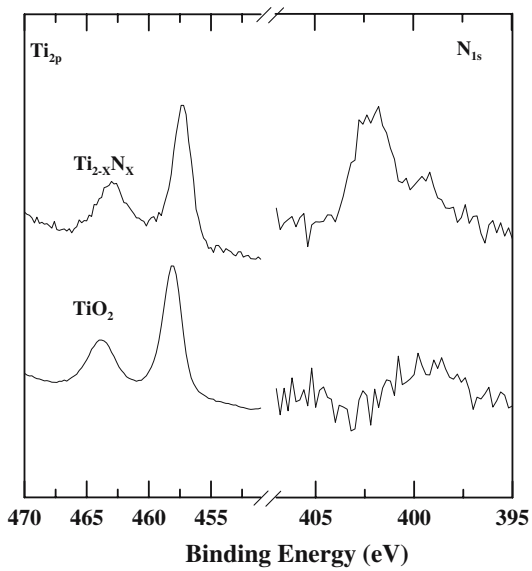

Figure 5. ESCA spectra of Ti 2p and N 1s that show evidence of nitrogen doping into the TiO_2 photocatalyst.

These feature peaks at 400–402 eV were assigned either to be bound to hydrogen (Diwald et al., 2004), to the chemisorbed γ-N_2 (Yang et al., 2004a) or to the formation of oxynitride (Chen et al., 2005) as the N-doping status. For examples, Diwald et al. (2004) showed that the peak observed at 399.6 eV is responsible for the shift of the photochemical threshold down to ~2.4 eV. And this form of nitrogen is most likely located in an interstitial site bound to hydrogen. Diwald et al. (2004) also indicated that this form of nitrogen doping disagrees with the conclusion of Asahi et al. (2001), who reported that nitride ions that substitute for O^{2-} ions in the TiO_2 lattice are the necessary dopant species for TiO_2 photocatalysis in the visible-light region. Chen and Burda (2005) assigned the N_{1s} peak observed at 402 eV to O–Ti–N formation, which can also enhance the photocatalytic activity in visible light region. In reference to literature data, it revealed that N-doping sites other than TiN observed at N 1s of 396 eV could also be responsible for effective photocatalysis in the visible light region.

Photocatalytic activity of N-doped TiO_2 in a batch reactor

The extent of IPA photocatalysis to form acetone vapors was tested in a batch-type reactor exposed under both 10 W of UV (Figure 6a) and visible light (Figure 6b) illumination. One can observe from Figure 6a that near complete removals of IPA was achieved in about 20 min by both bare TiO_2 and N-doped TiO_2. The peak concentrations of acetone were observed at around 8 min before the complete destruction of IPA and the acetone concentrations gradually approached zero at around 30 min.

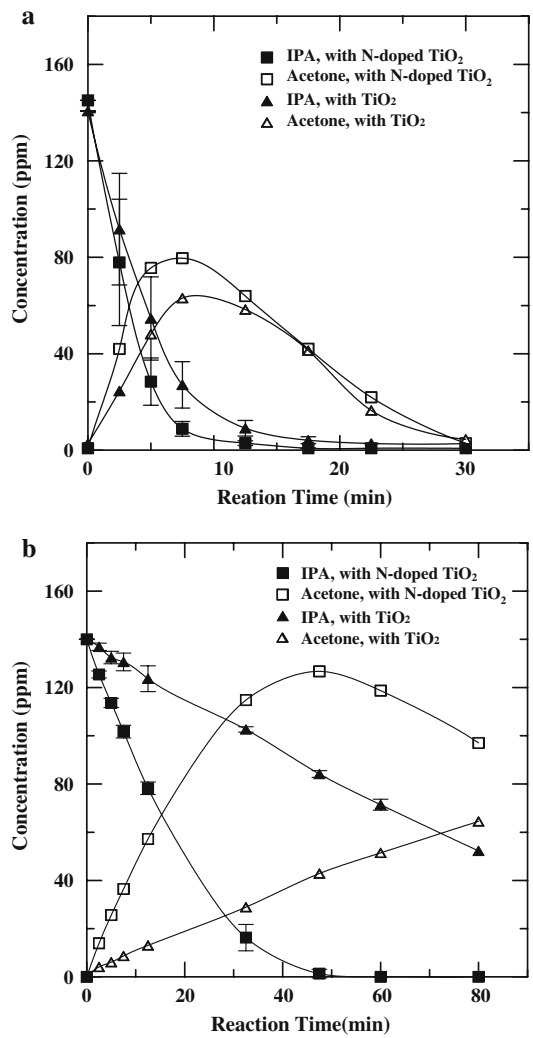

Figure 6. (a) The decomposition of IPA and the formation of acetone as a function of time in a batch photocatalytic reactor under UV light (10 W, peak at 364.2 nm). (b) The decomposition of IPA and the formation of acetone as a function of time in a batch photocatalytic reactor under visible light (10 W, peaks at 435, 488, 545, 587 and 611 nm).

On the other hand, as observed in Figure 6b the IPA and acetone removal rates were much slower under visible light irradiation when compared to the UV light irradiation. For test with N-doped TiO_2, near complete destruction of IPA was achieved at around 50 min. The formation of acetone also reached its peak concentration at the same time and then the acetone concentration started to decay. While for test with bare TiO_2, the IPA oxidation was still undergoing even after 80 min of irradiation.

In comparison of Figure 6a and b, one can see that under UV-irradiation where acetone could be oxidized to CO_2 even though the IPA destruction had not yet been completed. But this was not the case under visible light irradiation; the destruction of acetone would occur only after the IPA had been completely oxidized. Thus the visible light photocatalysts may be good for organics degradation but they may require much longer time for mineralization (total oxidation to CO_2).

Even though the bare anatase TiO_2 showed less photocatalytic activity than the N-doped TiO_2 in the visible light source, it was still photocatalytic effective in the visible light range. This may be different from typical understanding that bare anatase TiO_2 should be non-effective in the visible light range. But since photocatalytic tests with 364.2 nm UV lamb at the intensity of 0.43 mW/cm^2 showed negligible photo-activity, it was not due to the minor UV peak (0.35 mW/cm^2 at 364 nm) of the visible light lamb for this photo-activity. This phenomenon was also observed in the literature, for examples, Asahi et al. (2001) and Nosaka et al. (2005) used color filters to filter out the UV light source and conducted bare anatase TiO_2 for photocatalytic tests under visible light range. They still found some photo-activity for the bare anatase TiO_2 in the visible light range.

In order to study the visible-light induced photocatalysis of odorous VOCs with another representative molecular structure (i.e., aromatic ring), the photocatalytic removals of toluene vapors via the N-doped TiO_2 and the bare TiO_2 in a batch reactor were also tested and the results are shown in Figure 7 under both UV and visible light illumination. One can see that the N-doped TiO_2 had higher activities than bare TiO_2 under both UV and visible light sources. But at an initial time of less than 10 min, the removal rates of toluene were almost the same using the same photocatalyst

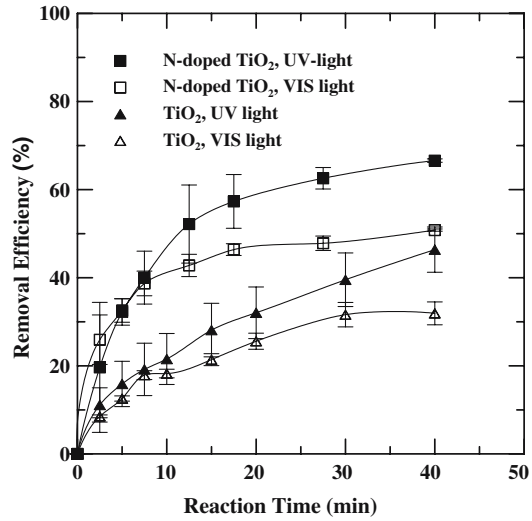

Figure 7. The removal efficiency of toluene as a function of time in a batch photocatalytic reactor under UV (10 W, peak at 364.2 nm) and visible light (10 W, peaks at 435, 488, 545, 587 and 611 nm) sources.

under the same light intensity and were almost independent of the light source. Then after 10 min of reaction time, the difference on the toluene removals between UV and visible light sources was increased. The toluene removal rates under visible light source were gradually retarded for both N-doped TiO_2 and bare TiO_2. This might be caused by the formation of intermediate species such as benzoic acid, benzyl alcohol and benzaldehyde during the decomposition of toluene vapors. Such intermediate products which strongly adsorbed were less reactive on the catalysts surface and led to deactivation of the catalyst (d'Hennezel et al., 1998).

Comparison of N-doped TiO_2 photocatalysis with commercial photocatalysts

The extent of decomposition of toluene vapor in a continuous-flow reactor with a short residence time of 2.35 min was evaluated to explore other application field such as air cleaners. The comparison results of photocatalytic activity between the N-doped TiO_2 produced in this study and the commercial photocatalysts of P25 and ST01 are shown in Figure 8. One can see that the toluene removal efficiency for N-doped TiO_2 gradually increased with the operation time of the continu-

ous flow reactor. It then reached a near steady-state removal efficiency of around 7.5% ± 0.5%. On the other hand, the toluene removal efficiencies of both ST01 and P25 were less than that of the N-doped TiO_2. Although the toluene removal efficiency of ST01 was slightly higher than that of P25, the difference in the removal efficiency was within 2%. With the relative reactivity of P25 photocatalyst (0.125 μmole/h), defined by the accumulated amount of toluene removal over 60 min of operation, as the reference base (relative reactivity = 1), it was calculated that the photoactivity of ST01 photocatalyst was approximately 3.2 times higher than that of the P25 photocatalyst. The relative activity for the N-doped photocatalyst prepared in this study, in comparison, was notably greater than both commercial photocatalysts, with reactivity of 11.2 and 3.5 times higher than those of P25 and ST01 photocatalysts, respectively.

Very limited literature data have compared the visible-light induced photocatalytic activity of the N-doped TiO_2 with those of the commercial photocatalysts. Li et al. (2005a, 2005b) prepared the N-doped and N-F-codoped TiO_2 photocatalysts via spray pyrolysis and demonstrated that the photocatalytic activities of N-doped and N-F-codoped TiO_2 were about 2 and 7 times, respectively, higher than that of the P25 photocatalyst in terms of the initial removal rate of acetaldehyde using a 150 W Xe lamp visible light source with 420 nm cut filter. Chen et al. (2005) prepared nanocolloid N-doped photocatalysts via a liquid phase method and found that the photocatalytic activity of the nanocolloid N-doped photocatalyst was 7 times higher than that of the P25 photocatalyst in terms of the methylene blue decomposition with a 540 nm visible light source. Our test result on comparing the visible light-driven photocatalytic activity of the N-doped photocatalyst and the commercial P25 was qualitatively similar to those by Li et al. (2005b) and Chen et al. (2005) prepared via other processes. In addition, the N 1s spectra of N-doped TiO_2 reported in this study was also very similar to those prepared by Chen et al. (2005), both exhibiting peaks at around 400–402 eV.

The Kubelka–Munk absorption spectra (Francisco et al., 2000) of N-doped TiO_2, ST01 and P25 were shown in Figure 9, and they showed that the UV-visible spectra of N-doped TiO_2, ST01 and P25 were consistent with their toluene removal efficiency. As observed that the N-doped TiO_2 prepared in this study has a clear red shift into the visible light absorption range, with two absorption

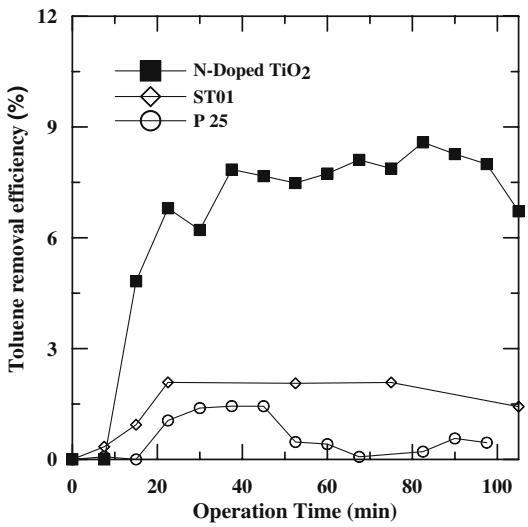

Figure 8. Comparison of the toluene decomposition between P25, ST01 and the N-doped TiO_2 ($TiO_{2-x}N_x$) photocatalysts tested in a continuous flow reactor under visible light (10W) illumination. The residence time in the reactor was 2.35 min.

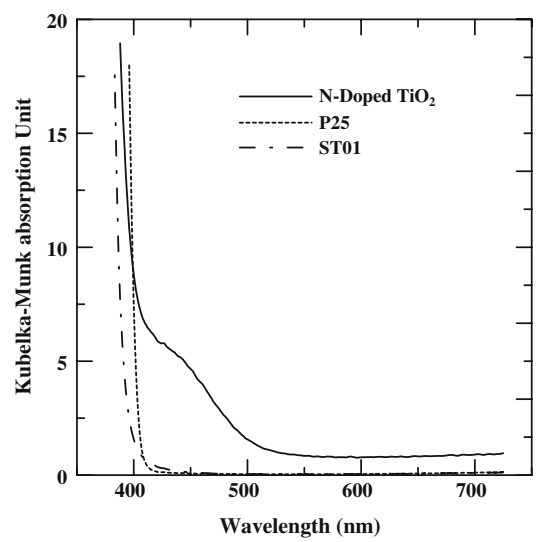

Figure 9. Kubelka-Munk absorption spectra of the commercial photocatalysts (P25 and ST01) and the N-doped TiO_2 ($TiO_{2-x}N_x$) photocatalyst prepared in this study.

edges at around 400 and 520 nm. On the other hand, there was only one absorption edge at around 395 and 405 nm, respectively, for the ST01 and the P25 photocatalysts. Also, although the wavelength of the absorption edge of P25 was slightly larger than that of ST01, their removal efficiencies were very similar ($< 2\%$) in the visible light range as demonstrated in Figure 8. This might be due to that the photocatalytic activity was also influenced by many other factors such as crystalline size, surface and bulk defects, porosity, surface area, impurities and active sites such as Ti^{3+} and OH sites etc.

Conclusion

The N-doped TiO_2 was prepared in this study via the APPENS process. The advantages of the APPENS process, as compared to other plasma processes for producing N-doped TiO_2 films or particles, encompass operation under normal temperature and pressure, as well as possessing a higher film deposition rate with lower power consumption. Effective removal of odorous VOCs in both batch and continuous flow photocatalytic reactors under visible and UV light sources were demonstrated as well. The results showed that the N-doped TiO_2 photocatalyst was more effective in removing IPA under both UV and visible light sources than the un-doped TiO_2 photocatalyst. Furthermore, the N-doped TiO_2 photocatalyst was superior in toluene removal than the commercial ST01 and P25 TiO_2 photocatalysts under visible light irradiation. Considering that UV light accounts for only 3–5% of the solar light intensity, and that indoor lighting is predominantly in the visible light range, the results presented in this study strongly suggest that the N-doped TiO_2 photocatalysts prepared via the APPENS process has a potential application in the arena of indoor and outdoor air pollution control.

Acknowledgments

The authors acknowledge the supports from the National Science Council, Taiwan, through grant numbers NSC 91-2211-E-009-012, 92-2211-E-009-017 and 93-2211-E-009-018.

References

Asahi R., T. Morikawa, T. Ohwaki, K. Aoki & Y. Taga, 2001. Visible-light photocatalysis in nitrogen-doped titanium oxides. Science 293, 269–271.

Bai H., C. Chen, C.-H. Lin, W. Den & C. Chang, 2004. Monodisperse nanoparticle synthesis by an atmospheric pressure plasma process: an example of a visible light photocatalyst. Industrial Eng. Chem. Res. 43, 7200–7203.

Battison G.A., R. Gerbasi, A. Gregori, M. Porchia, S. Cattarin & G.A. Rizzi, 2000. PECVD of amorphous TiO_2 thin films: effect of growth temperature and plasma gas composition. Thin Solid Films 371, 126–131.

Chen X., Y. Lou, A.C.S. Samia, C. Burda & J.L. Gole, 2005. Formation of oxynitride as the photocatalytic enhancing site in nitrogen-doped titania nanocatalysts: comparison to a commercial nanopowder. Adv. Funct. Mat. 15, 41–49.

Chen X. & C. Burda, 2004. Photoelectron spectroscopic investigation of nitrogen-doped titania nanoparticles. J. Phys. Chem. B 108, 15446–15449.

d'Hennezel O., P. Pichat & D.F. Ollis, 1998. Benzene and toluene gas-phase photocatalytic degradation over H_2O and HCl pretreated TiO_2: by products and mechanisms. J. Photochem. Photobiol. A 118, 197–204.

Diwald O., L.T. Tracy, Z. Tykhon, G. Goralski, D. Scott Walck & T. John Yates Jr., 2004. Photochemical activity of nitrogen-doped rutile $TiO_2(110)$ in visible light. J. Phys. Chem. B 108, 6004–6008.

Francisco H.I., R.S. Berns & Di-Y. Tzeng, 2000. A comparative analysis of spectral reflectance estimated in various spaces using a trichromatic camera system. J. Imaging Sci. Technol. 44, 280–287.

Fujishima A., T.N. Rao & D.A. Tryk, 2000. Titanium dioxide photocatalysis. J. Photochem. Photobiol. C 1, 1–21.

György E., A.P. del Pino, Serra & J.L. Morenza, 2003. Depth profiling characterisation of the surface layer obtained by pulsed Nd:YAG laser irradiation of titanium in nitrogen. Surf. Coat. Technol. 173, 265–270.

Ihara T., M. Miyoshi, Y. Iriyama, M. Matsumoto & S. Sugihara, 2003. Visible-light-active titanium oxide photocatalyst realized by an oxygen-deficient structure and by nitrogen doping. Appl. Catal. B 42, 403–409.

Irie H., Y. Watanabe & K. Hashimoto, 2003. Nitrogen-Concentration Dependence on Photocatalytic Activity of $TiO_{2-x}N_x$ Powders. J. Phys. Chem. B 107, 5483–5486.

Jill, C. (Ed.), 1992. Handbook of X-ray Photoelectron Spectroscopy. Minnesota: Perkin–Elmer Corporation 43.

Li D., H. Haneda, S. Hishita & N. Ohashi, 2005a. Visible-light-driven N-F-codoped TiO_2 Photocatalysts. 2. Optical characterization, photocatalysis, and potential application to air purification. Chem. Mat. 17, 2596–2602.

Li D., H. Haneda, S. Hishita & N. Ohashi, 2005b. Visible-light-driven nitrogen-doped TiO_2 photocatalysts: effect of nitrogen precursors on their photocatalysis for decomposition of gas-phase organic pollutants. Mat. Sci. Eng. B 117, 67–75.

Livraghi S., A. Votta, M.C. Paganini & E. Giamello, 2005. The nature of paramagnetic species in nitrogen doped TiO_2 active in visible light photocatalysis. Chem. Commun. 4, 498–500.

Maeda M. & T. Watanabe, 2006. Visible light Photocatalysis of Nitrogen-diped oxide films prepared by plasma-enhanced chemical vapor deposition. J. Electrochem. Soc. 153(3), C187–C189.

Miao L., S. Tanemura, H. Watanabe, Y. Mori, K. Kaneko & S. Toh, 2004. The improvement of optical reactivity for TiO_2 thin films by N_2-H_2 plasma surface-treatment. J. Crystal Growth 260, 118–124.

Musić S., Gotić M., M. Ivanda, Popvić S., Turković A., R. Trojko, Sekulić A. & K. Furić, 1997. Chemical and microstructural properties of TiO_2 synthesized by sol–gel procedure. Mat. Sci. Eng. B 47, 33–40.

Nosaka Y., M. Matsushita, J. Nishino & A.Y. Nosaka, 2005. Nitrogen-doped titanium dioxide photocatalysts for visible response prepared by using organic compounds. Sci. Technol. Adv. Mat. 6, 143–148.

Ohno T., M. Akiyoshi, T. Umebayashi, K. Asai, T. Mitsui & M. Matsumura, 2004. Preparation of S-doped TiO_2 photocatalysts and their photocatalytic activities under visible light. Appl. Catal. A 265, 115–121.

Sakatani Y., H. Ando, K. Okusako & H. Koike, 2004. Metal ion and N co-doped TiO_2 as a visible-light photocatalyst. J. Mat. Res. 19, 2100–2108.

Suda Y., H. Kawasaki, T. Ueda & T. Ohshima, 2005. Preparation of nitrogen-doped titanium oxide thin film using a PLD method as parameters of target material and nitrogen concentration ratio in nitrogen/oxygen gas mixture. Thin Solid Films 475, 337–341.

Wu P.-G., C.-H. Ma & J.K. Shang, 2005. Effects of nitrogen doping on optical properties of TiO_2 thin films. Appl. Phys. A 81, 1411–1417.

Yang M.-C., T.-S. Yang & M.-S. Wong, 2004a. Nitrogen-doped titanium oxide films as visible light photocatalyst by vapor deposition. Thin Solid Films 469(-470), 1–5.

Yang T.-S., C.-B. Shiu & M.-S. Wong, 2004b. Structure and hydrophilicity of titanium oxide films prepared by electron beam evaporation. Surf. Sci. 548, 75–82.

Yin S., Y. Aita, M. Komatsu, J. Wang, Q. Tang & T. Sato, 2005. Synthesis of excellent visible-light responsive $TiO_{2-x}N_y$ photocatalyst by a homogeneous precipitation-solvothermal process. J. Mat. Chem. 15, 674–682.